AUTOPHAGY
2023, VOL. 19, NO. 3, 945–956
https://doi.org/10.1080/15548627.2022.2111635

Taylor & Francis
Taylor & Francis Group

BRIEF REPORT

TMEM164 is a new determinant of autophagy-dependent ferroptosis

Jiao Liu[a,b], Yang Liu[a,b], Yuan Wang[a,b], Changfeng Li[c], Yangchun Xie[d], Daniel J. Klionsky[e], Rui Kang[f], and Daolin Tang[f]

[a]The DAMP Lab, The Third Affiliated Hospital, Guangzhou Medical University, Guangzhou, China; [b]Guangzhou Municipal and Guangdong Provincial Key Laboratory of Protein Modification and Degradation, Guangzhou Medical University, Guangzhou, China; [c]Department of Endoscopy Center, China-Japan Union Hospital of Jilin University, Changchun, China; [d]Department of Oncology, The Second Xiangya Hospital, Central South University, Changsha, China; [e]Life Sciences Institute and Department of Molecular, Cellular and Developmental Biology, University of Michigan, Ann Arbor, MI, USA; [f]Center for DAMP Biology, Department of Surgery, UT Southwestern Medical Center, Dallas, TX, USA

ABSTRACT

Macroautophagy (hereafter "autophagy") is a membrane-mediated biological process that involves engulfing and delivering cytoplasmic components to lysosomes for degradation. In addition to autophagy's pro-survival effect during nutrient starvation, excessive activation of autophagy machinery can also cause regulated cell death, especially iron-dependent ferroptosis. Here, we report a key role of TMEM164 (transmembrane protein 164) in selectively mediating ATG5 (autophagy related 5)-dependent autophagosome formation during ferroptosis, rather than during starvation. In contrast, the membrane protein ATG9A (autophagy-related 9A) is dispensable for the formation of autophagosomes during ferroptosis. TMEM164-mediated autophagy degrades ferritin, GPX4 (glutathione peroxidase 4), and lipid droplets to increase iron accumulation and lipid peroxidation, thereby promoting ferroptotic cell death. Consequently, the loss of TMEM164 limits the anticancer activity of ferroptosis-mediated cytotoxicity in mice. High TMEM164 expression is associated with improved survival and increased immune cell infiltration in patients with pancreatic cancer. These findings establish a new mode of autophagy-dependent ferroptosis.

ARTICLE HISTORY
Received 8 April 2022
Revised 3 August 2022
Accepted 4 August 2022

KEYWORDS
Autophagy; cell death; ferroptosis; membrane protein; tumor immunity

Introduction

Ferroptosis is a type of iron-dependent regulated cell death that plays a context-dependent role in health and disease [1,2]. Modulating the activities of ferroptosis holds promise for cancer treatment [3]. In addition to mammalian cells, ferroptosis has also been detected in plants following heat stress [4], indicating that this cell death modality may be a conserved process. Generally, the induction of ferroptosis involves an imbalance between oxidative stress and antioxidant defense, which ultimately leads to lipid peroxidation, plasma membrane damage, and the release of danger/damage-associated molecular patterns (DAMPs) [5,6]. The classical ferroptosis inducers are inhibitors of the antioxidant SLC7A11 (solute carrier family 7 member 11)-GPX4 (glutathione peroxidase 4) axis [7]. Several regulated cell death effectors, such as caspases, MLKL (mixed lineage kinase domain like pseudokinase) and GSDMD (gasdermin D), are not necessary for ferroptosis [8], highlighting the uniqueness of the execution of this pathway.

Macroautophagy (hereafter "autophagy") is a lysosomal-dependent degradation process, by which the recycling of cellular material can promote survival under various environmental stresses, especially nutritional deprivation [9,10]. In contrast, unrestricted autophagy may lead to cell death by selectively degrading survival-promoting molecules or organelles. Autophagy is regulated and executed by a group of conserved proteins called ATG (autophagy related) proteins, which form different complexes to shape membrane dynamics to engulf and degrade the cargoes [11]. Recently, ferroptosis was recognized as a form of autophagy-dependent cell death and the depletion of core components of autophagic machinery, such as ATG5, ATG7, and BECN1/Vps30/Atg6 (beclin 1), inhibits ferroptotic cell death [12–21]. Autophagy-induced signaling during ferroptosis is associated with oxidative stress and iron accumulation, and excessive autophagy can feedback accelerate these signals understood [22,23]. Although these advances in knowledge are significant, the selective process and regulation of autophagy-dependent ferroptosis are still poorly.

TMEM164 (transmembrane protein 164) is a member of the transmembrane protein (TMEM) family that spans various biological membranes, including the plasma membrane and the membrane of organelles [24]. The Xq22.3q23 microdeletion containing the *TMEM164* gene is associated with Alport syndrome, intellectual disability, midfacial hypoplasia, and elliptocytosis [25,26]. The changes in the *TMEM164* gene and other TMEM members are independent factors affecting the prognosis of lung adenocarcinoma [27]. Although TMEM164 is a highly conserved protein, its function remains unknown.

In this study, we analyzed the data of a clustered regularly interspaced short palindromic repeat (CRISPR)-Cas9 (CRISPR-associated protein 9) library screening from a previous study that used the small molecule compound ML210 to trigger ferroptosis in human kidney cancer cells [28]. This genetic screen indicated that TMEM164 is one of

CONTACT Jiao Liu 2018683073@gzhmu.edu.cn 5323 Harry Hines Blvd, Department of Surgery, UT Southwestern Medical Center, Dallas, TX 75390, USA; Daolin Tang daolin.tang@utsouthwestern.edu No. 63, Duobao Road, Liwan District, The Third Affiliated Hospital, Guangzhou Medical University, Guangzhou 510150, China

the top candidate genes for promoting ferroptosis. Our function and mechanism studies further revealed that TMEM164 plays a key role in promoting autophagy-dependent ferroptosis by sustaining autophagosome formation. In contrast, TMEM164 is dispensable for classical starvation-induced autophagosome formation.

Results

TMEM164 acts as a promoter of ferroptosis

CRISPR-Cas9 genetic screening provides a valuable approach to reveal the new genetic dependence of ferroptosis. We analyzed a genome-scale CRISPR-Cas9 knockout screening study in 786-O cells (a human clear cell, renal carcinoma cell line) during ferroptosis triggered by the chemical ML210 [28]. In addition to the well-characterized ferroptosis promoters ACSL4 (acyl-CoA synthetase long chain family member 4) [29–31] and POR (cytochrome p450 oxidoreductase) [32,33], TMEM164 was identified as one of top hits (Figure 1A), highlighting a potential role of TMEM164 in regulating ferroptosis.

To determine whether TMEM164 is required for ferroptosis, we utilized shRNA-mediated RNA interference (RNAi) to inhibit the expression of TMEM164 in HT1080 cells (a human fibrosarcoma cell line) and PANC1 cells (a human pancreatic ductal adenocarcinoma cell line), which are widely used in the study of ferroptosis mechanisms [34–37]. The suppression of *TMEM164* expression by two different shRNAs (Figure 1B) blocked SLC7A11 inhibitors (e.g., erastin, sulfasalazine, and sorafenib)- or GPX4 inhibitors (e.g., RSL3, ML162, and ML210)-induced cell death (Figure 1C). In contrast, the loss of *TMEM164* had no significant effects on cell death due to the apoptosis inducer staurosporine or the necroptosis trigger CCT137690 (Figure 1C) [38]. Thus, TMEM164 appears be a specific regulator of ferroptosis, but not apoptosis and necroptosis.

To further examine the effects of TMEM164 in ferroptosis, we established an RSL3-resistant PANC1 cell line (termed $PANC1^R$) using a method involving stepwise dose escalation and the limiting of single-cell dilution. Western blot analysis revealed that the expression of TMEM164 was reduced in $PANC1^R$ cells (Figure 1D). We also examined other key ferroptosis regulators, such as GPX4 and SLC7A11, accordingly. The expression of SLC7A11 in $PANC1^R$ cells was not significantly changed compared to parental cells (Figure 1D). In contrast, GPX4 expression was upregulated in $PANC1^R$ cells compared to parental cells (Figure 1D). Ferroptosis-resistant cells have aberrant expression of many genes [39], mainly regulated by the antioxidant transcription factor NFE2L2/NRF2 (NFE2 like BZIP transcription factor 2) [40,41]. Brusatol, an NFE2L2 inhibitor [42], inhibited *TMEM164* mRNA expression in $PANC1^R$ cells (Figure 1E), supporting the role of NFE2L2 in negatively regulating TMEM164 gene expression.

Compared to the parental cell line, $PANC1^R$ cells were capable of maintaining viability with continuous exposure to RSL3 at 10 μM (Figure 1F). In contrast, the gene transfection-mediated overexpression of *TMEM164* restored the sensitivity of $PANC1^R$ cells (termed $PANC1^{R164}$ cells; Figure 1D) to RSL3, and this process was inhibited by the ferroptosis inhibitor liproxstatin-1 (Figure 1F). The overexpression of *TMEM164* reduced GPX4 expression in $PANC1^R$ cells (Figure 1D), suggesting a negative expression correlation between TMEM164 and GPX4 in $PANC1^R$ cells.

We next examined the effects of TMEM164 on characteristic biochemical events of ferroptosis, including iron accumulation and lipid peroxidation. Quantitative analysis of intracellular ferrous ions (Fe^{2+}) and malondialdehyde (MDA, an endogenous genotoxic product of lipid peroxidation) revealed that the knockdown of *TMEM164* inhibited erastin- or RSL3-induced Fe^{2+} accumulation and lipid peroxidation in PANC1 cells (Figure 1G,H). As expected, the release of a prototypical DAMP, namely the molecule HMGB1 (high mobility group box 1) [43], during ferroptosis was also inhibited by the knockdown of *TMEM164* (Figure 1I). Altogether, these findings demonstrate that TMEM164 is a positive regulator of ferroptosis.

TMEM164 promotes ferroptosis by activating autophagy

To study the mechanism and action of TMEM164 in ferroptotic cell death, we determined the effect of TMEM164 silencing on the expression of proteins responsible for the repair of lipid peroxides, including GPX4 [44], AIFM2/FSP1 (apoptosis inducing factor mitochondria associated 2) [45,46], and DHODH (dihydroorotate dehydrogenase (quinone)) [47]. Compared to AIFM2 and DHODH, the protein expression of GPX4 was reduced by erastin or RSL3 in PANC1 cells (Figure 2A). The loss of *TMEM164* reduced the downregulation of GPX4 protein during ferroptosis (Figure 2A). TMEM164 had no significant effects on the protein expression of AIFM2 and DHODH (Figure 2A) as well as the mRNA of *GPX4* (Figure 2B). These data indicate that TMEM164 selectively regulates GPX4 protein degradation during ferroptosis.

Because GPX4 is a degradative substrate of autophagy in ferroptosis [36,48], we evaluated whether other autophagic substrates are also affected by TMEM164. We focused on ferritin and lipid droplets because the autophagic degradation of ferritin by ferritinophagy [12,13] or lipid droplets by lipophagy [49] favors iron accumulation and/or lipid peroxidation during ferroptosis. The knockdown of *TMEM164* prevented erastin- or RSL3-induced downregulation of the protein expression of FTH1 (ferritin heavy chain 1) (Figure 2A). The measurement of lipid droplets also revealed that erastin- or RSL3-induced lipid droplet degradation requires TMEM164 (Figure 2C). Similar to the knockdown of *TMEM164*, shRNA-mediated *ATG5* RNAi prevented the degradation of GPX4, FTH1, and lipid droplets in PANC1 cells after treatment with erastin or RSL3 (Figure 2A,C). Bafilomycin A_1, an inhibitor of autophagosome-lysosome fusion [50], also increased FTH1 and GPX4 expression, as well as decreased Fe^{2+} accumulation in response to erastin or RSL3 (Figure 2D,E).

Because the degradation of GPX4, FTH1, and lipid droplets requires different autophagy receptors [12,13,48,49], we hypothesized that TMEM164 may affect the upstream formation of autophagosomes rather than by directly recognizing

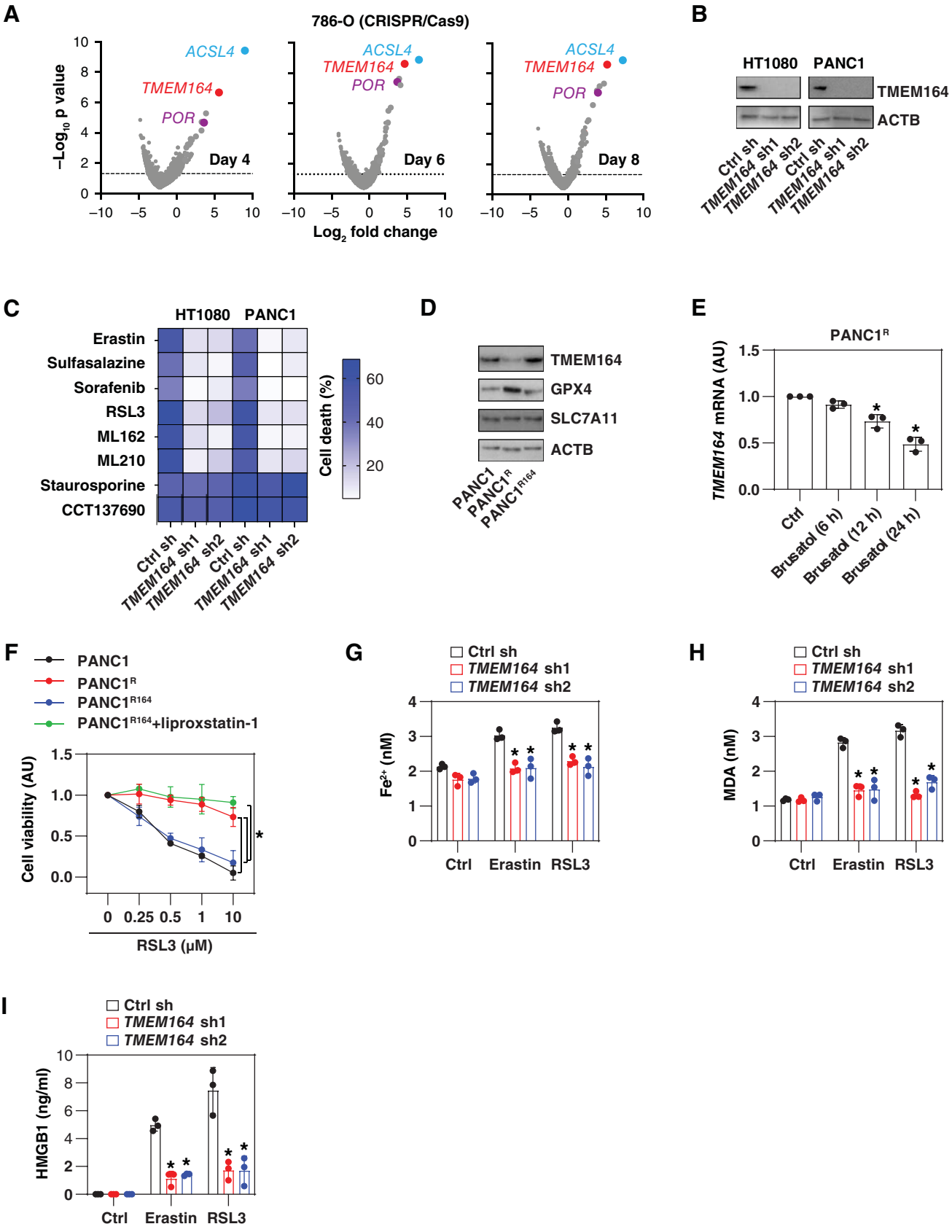

Figure 1. TMEM164 acts as a promoter of ferroptosis. (A) Partial volcano plots highlighting ACSL4, TMEM164, and POR as the top hits in a previous genome-wide screen using CRISPR-Cas9 in ML210-induced 786-O cells [28]. (B) Western blot analysis of TMEM164 expression in the indicated *TMEM164*-knockdown HT1080 and PANC1 cells. (C) Cell death assay in the indicated HT1080 and PANC1 cells following treatment with erastin (5 μM), sulfasalazine (500 μM), sorafenib (10 μM), RSL3 (0.5 μM), ML162 (0.5 μM), ML210 (5 μM), staurosporine (200 nM), or CCT137690 (5 μM) for 24 h (data are shown in a heat map as the means of 3 biologically independent samples). (D) Western blot analysis of TMEM164 expression in control PANC1, RSL3-resistant PANC1 (PANC1^{R}), or TMEM164-overexpressed PANC1^{R} (PANC1^{R164}) cells. (E) qPCR analysis of *TMEM164* mRNA in PANC1^{R} cells following treatment with brusatol (100 nM) for 6–24 h ($n = 3$ biologically independent samples; *$P < 0.05$, one-way ANOVA with Tukey's multiple comparisons test; data are presented as means ± SD). (F) Cell viability in the indicated PANC1 cells following treatment with RSL3 (0.25–

cargoes. In fact, the knockdown of TMEM164 inhibited the formation of MAP1LC3B/LC3 (microtubule associated protein 1 light chain 3 beta)-II based on immunoblotting measurement (Figure 2A) or MAP1LC3B puncta assessed by immunofluorescence analysis (Figure 2F) following RSL3 treatment, but not in response to Hanks' balanced salt solution (HBSS)-induced starvation. As a control, knockdown of *ATG9A*, a multi-spanning membrane protein essential for autophagosome formation during starvation [51–53], had the reverse effect, inhibiting MAP1LC3B puncta formation in response to HBSS, but not RSL3 (Figure 2F). An autophagy flux assay using a GFP-LC3-RFP-LC3ΔG probe [54] relies on the stable fluorescence of RFP, but quenching of GFP, within the lysosome following autophagosome-lysosome fusion. This microplate reader assay similarly revealed that the knockdown of *TMEM164* or *ATG9A* impaired only RSL3-induced or HBSS-induced autophagic flux, respectively (Figure 2G). Confocal microscopy assays further confirmed that the knockdown of *TMEM164* inhibited RSL3-induced accumulation of LC3 puncta in PANC1 cells by the GFP-LC3-RFP-LC3ΔG construct (Figure 2H).

ATG5 is essential for autophagosome formation through the formation of the ATG12–ATG5-ATG16L1 complex [55,56]. The loss of *TMEM164* reduced the binding between ATG5 and ATG16L1 in response to RSL3, but not the stimulation from HBSS (Figure 2I). In contrast, the shRNA-mediated knockdown of *ATG9A* had no effect on the RSL3-stimulated increase in ATG5-ATG16L1 complex formation (Figure 2J). In contrast to the knockdown of *TMEM164*, the silencing of *ATG9A* failed to block RSL3-induced cell viability inhibition (Figure 2K). The overexpression of *Tmem164* failed to restore MAP1LC3B-II expression in *atg5*$^{-/-}$ MEFs in the absence or presence of RSL3 (Figure 2L). Collectively, these findings underscore a special upstream role of TMEM164 (but not ATG9A) in the production of ATG5-dependent autophagosomes for ferroptosis.

Next, we examined which autophagy substrate is critical for TMEM164-mediated ferroptosis. The knockdown of *GPX4* restored the sensitivity of *TMEM164*-knockdown PANC1 cells to ferroptosis more than the knockdown of *FTH1* or the administration of pyrrophenone (Figure 2M, an inhibitor of lipid droplet formation [57]). Thus, GPX4 may be the most important autophagic degradation substrate for TMEM164-mediated ferroptosis, although other substrates also contribute to this process.

TMEM164 mediates the anticancer activity of RSL3 in vivo

To evaluate the effects of TMEM164-mediated ferroptosis *in vivo*, we used a PANC1-derived xenograft model in immunodeficient NOD SCID mice. Compared with the control group, the anticancer activity of RSL3 was limited in the *TMEM164*-knockdown (*TMEM164* KD) PANC1 group (Figure 3A). Subsequent analysis of ferroptosis markers (including the mRNA of *PTGS2* [prostaglandin-endoperoxide synthase 2] or *ACSL4*) (Figure 3B,C), iron accumulation (Figure 3D), MDA levels (Figure 3E), and ACSL4 production 5-hydroxyeicosatetraenoic acid (5-HETE; Figure 3F) confirmed the role of TMEM164 in promoting RSL3-induced ferroptosis in isolated tumors. In contrast, the activity of CASP3 (caspase 3) was not changed in the *TMEM164* KD group in the absence or presence of RSL3 (Figure 3G). Consistent with the finding that TMEM164 is required for autophagy-dependent ferroptosis *in vitro* (Figure 2), western blot analysis confirmed that RSL3-induced MAP1LC3B-II expression in isolated tumors was inhibited in the TMEM164 KD group (Figure 3H).

The role of TMEM164 expression in human pancreatic ductal adenocarcinomas

To determine clinical relevance of the experimental findings, the prognostic value of TMEM164 was evaluated in patients with pancreatic cancer using The Cancer Genome Atlas (TCGA) database. *TMEM164* mRNA was significantly upregulated in PDACs compared with normal pancreas tissues (Figure 4A). High levels of *TMEM164* mRNA were associated with improved survival (Figure 4B), suggesting that TMEM164 may exert a tumor suppressor effect in human pancreatic cancer. We next assayed the localization of TMEM164 protein expression in human pancreatic ductal adenocarcinomas from The Human Protein Atlas platform. Immunohistochemistry staining showed that the expression of TMEM164 was mainly confined to ductal cells in certain PDAC patients (Figure 4C). In addition, the Tumor IMmune Estimation Resource (TIMER) showed that the mRNA expression level of *TMEM164* was positively related to the infiltration of a variety of immune cells, especially cytotoxic CD8+ T cells, antigen-presenting dendritic cells, and cancer-associated fibroblasts (Figure 4D). In contrast, *TMEM164* was negatively related to the infiltration of cancer-associated fibroblasts (Figure 4D). These analyses suggest that TMEM164 plays a role in modulating the immune microenvironment of human pancreatic ductal adenocarcinomas.

Discussion

Autophagy is a highly integrated process that maintains cell homeostasis by promoting cell survival or causing cell death. Here, we demonstrated a key role of TMEM164 in driving autophagy-dependent ferroptotic cell death by promoting autophagosome formation during lipid peroxidation (Figure 5). These findings not only provide insights for understanding the degradation regulation mechanism of ferroptosis, but also suggest an alternative strategy to trigger antitumor immunity [58].

10 μM) for 24 h ($n = 3$ biologically independent samples; *$P < 0.05$, two-way ANOVA with Tukey's multiple comparisons test; data are presented as means ± SD). (G-I) Analysis of intracellular Fe^{2+} (G), intracellular MDA (H), and extracellular HMGB1 (I) in indicated control and *TMEM164*-knockdown PANC1 cells following treatment with erastin (5 μM) or RSL3 (0.5 μM) for 24 h ($n = 3$ biologically independent samples; *$P < 0.05$ versus control shRNA group, one-tailed *t* test; data are presented as means ± SD).

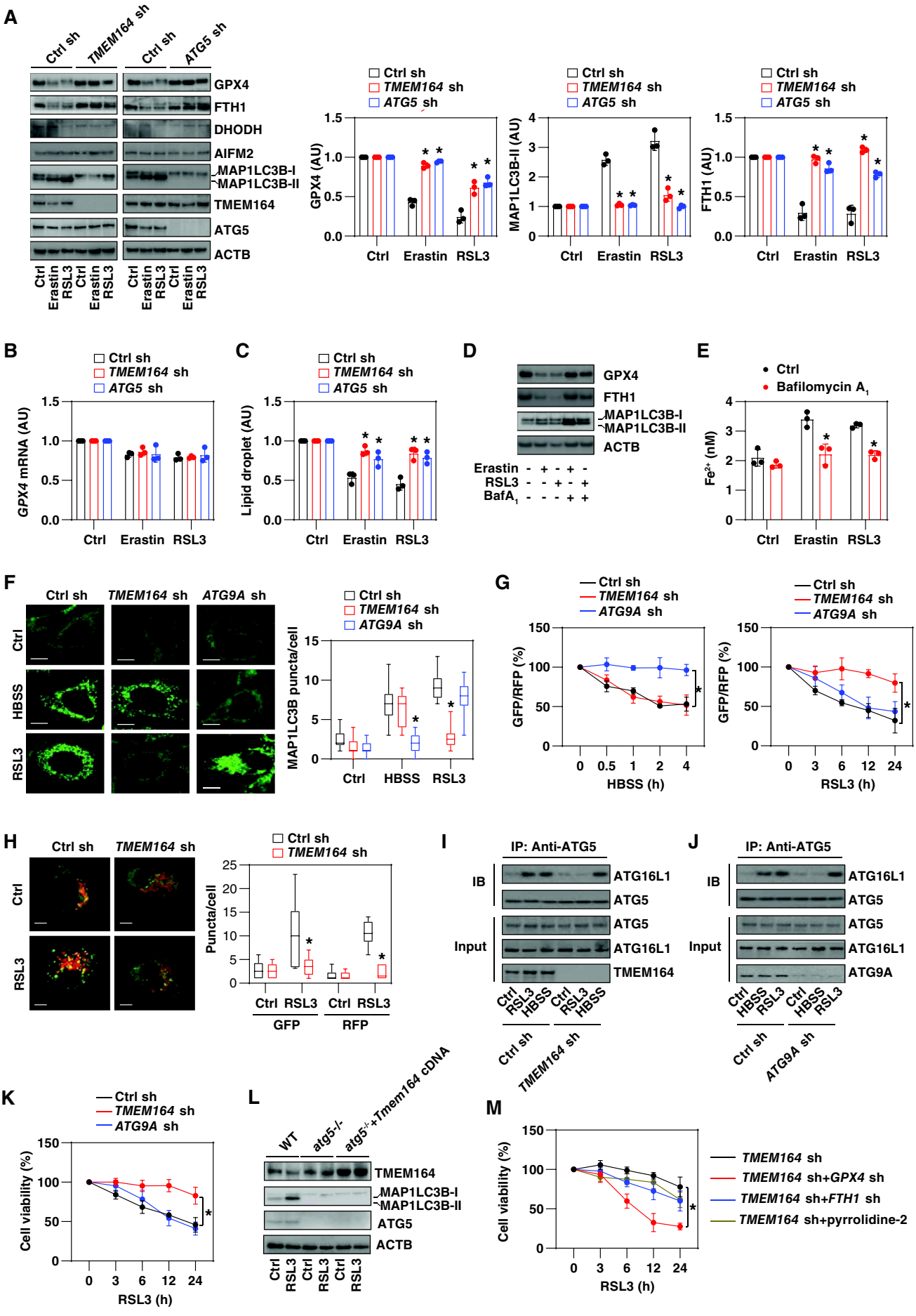

Figure 2. TMEM164 promotes ferroptosis by activating autophagy. (A) Western blot analysis of the indicated protein expression in *TMEM164*-knockdown or *ATG5*-knockdown PANC1 cells following treatment with erastin (5 μM) or RSL3 (0.5 μM) for 24 h. Relative protein quantification is shown in the right panel ($n = 3$ biologically

Dysregulated autophagy is related to various cell death modalities [59]. Historically, the phrase "autophagic cell death" was used to morphologically define a type of cell death that accompanies large-scale autophagic vacuolization of the cytoplasm [60]. Today, a related phrase, "autophagy-dependent cell death", is used to functionally define a type of cell death that mechanistically relies on the autophagic machinery (or its components) [61]. Our knowledge of ferroptosis as an autophagy-dependent form of cell death provides an example for understanding the selective degradation mechanism that promotes cell death [62]. For example, the autophagic degradation of ferritin [12,13], the circadian clock protein BMAL1/ARNTL (basic helix-loop-helix ARNT like 1) [63], lipid droplets [49], the iron transporter SLC40A1/ferroportin (solute carrier family 40 member 1) [62], GPX4 [36,48], or CDH2 (cadherin 2) [64] enhances iron accumulation and/or reactive oxygen species/ROS production, leading to ferroptosis in a context-dependent manner.

Previous studies have shown that two important subtypes of autophagy (macroautophagy and chaperone-mediated autophagy) promote GPX4 degradation and ferroptosis [36,48], suggesting that subtypes of autophagic degradation of GPX4 may depend on cell type or stimulation. Our data suggest that autophagic degradation plays a major role in regulating GPX4 expression in PANC1 cells during ferroptosis. The knockdown of *ATG5* or the administration of bafilomycin A_1 restored erastin- or RSL3-induced GPX4 protein degradation to 80% compared to controls. Although we ruled out the possibility of regulating GPX4 at the transcriptional level, there are other possibilities (e.g., pre-transcriptional, post-transcriptional, pre-translational, translational and post-translational levels) that regulate GPX4 expression during ferroptosis [65,66]. In addition to different autophagy receptors responsible for ferroptosis [22], our current study shows that the regulation of autophagosome formation by TMEM164 during ferroptosis is distinct from classic starvation-induced autophagy.

Autophagy is a membrane-driven dynamic process involving the assembly, formation, and maturation of intracellular membrane structures, including phagophores, autophagosomes, and autolysosomes [11]. In mammalian cells, ATG9A is the transmembrane protein of the ATG family and has been proposed to play a key role in guiding the membranes of donor organelles to form autophagosomes during starvation [67]. Our current study shows that unlike ATG9A-dependent membrane acquisition, the transmembrane protein TMEM164 selectively participates in the ATG5-dependent autophagosome assembly process during ferroptosis. Although there are still many questions to be answered about the precise role of TMEM164 in controlling membrane dynamics, these new findings provide clues for elucidating the difference in autophagy mechanisms between starvation and ferroptosis.

Like the dysregulation of the autophagic-lysosomal pathway, ferroptosis plays a context-dependent role in cancer, and interventions to stimulate or inhibit ferroptosis have been proposed as cancer treatment or prevention [3]. For example, chronic inflammation caused by ferroptotic death can promote $Kras^{G12D}$-driven pancreatic tumorigenesis in mice [68]. In established tumors, drug-induced ferroptosis combined with other chemotherapy, radiotherapy, or targeted therapy has become an emerging anticancer strategy in preclinical tumor models [69–73]. The Xq22.3q23 microdeletion carrying the *TMEM164* and *ACSL4* genes is related to Alport syndrome and intellectual disability in humans [25,26], although it is not clear whether ferroptosis is related to these neurogenetic diseases. Our TCGA database analysis further supports the role of highly expressed TMEM164 in maintaining the anti-tumor immune environment of PDAC.

Together, our results reveal a previously unrecognized molecular link between autophagy and ferroptosis through the transmembrane protein TMEM164. Further understanding of the TMEM164-dependent autophagic process may guide the development of improved approaches and/or drugs for the treatment of ferroptosis-related diseases.

Materials and methods

Reagents

Erastin (S7242), sulfasalazine (S1576), sorafenib (S7397), RSL3 (S8155), CCT137690 (S2744), bafilomycin A_1 (S1413), brusatol (S7956), and liproxstatin-1 (S7699) were purchased from Selleck Chemicals. ML162 (20455), ML210 (23282), pyrrophenone (13294), and staurosporine (25096) were purchased from Cayman Chemical. The antibodies to FTH1 (4393), MAP1LC3B (3868), ATG5 (2630), ATG16L1 (8089), ATG9A (13509), SLC7A11 (12691) and ACTB (3700) were purchased from Cell Signaling Technology. The antibodies to TMEM164 (NBP1-93939) were purchased from Novus. The antibodies to

independent samples; *$P < 0.05$ versus control shRNA group, one-tailed *t* test; data are presented as means ± SD). (B, C) Analysis of *GPX4* mRNA and lipid droplet levels in the indicated gene knockdown PANC1 cells following treatment with erastin (5 μM) or RSL3 (0.5 μM) for 24 h ($n = 3$ biologically independent samples; *$P < 0.05$ versus control shRNA group, one-tailed *t* test; data are presented as means ± SD). (D) Western blot analysis of the indicated protein expression in PANC1 cells following treatment with erastin (5 μM) or RSL3 (0.5 μM) for 24 h in the absence or presence of bafilomycin A_1 ($BafA_1$; 20 nM) for 24 h. (E) Analysis of intracellular Fe^{2+} in PANC1 cells following treatment with erastin (5 μM) or RSL3 (0.5 μM) for 24 h in the absence or presence of bafilomycin A_1 (20 nM) for 24 h ($n = 3$ biologically independent samples; *$P < 0.05$ versus control group, one-tailed *t* test; data are presented as means ± SD). (F) Image analysis of MAP1LC3B puncta in the indicated gene knockdown PANC1 cells following treatment with HBSS (2 h) or RSL3 (0.5 μM, 12 h). The data are presented as box-and-whisker plots from 10 fields. Boxes represent the median and the 25th and 75th percentiles. *$P < 0.05$ versus control shRNA group, one-tailed *t* test; bar: 15 μm. (G) Analysis of the time course of relative GFP:RFP ratio in the indicated PANC1 cells expressing GFP-LC3-RFP-LC3ΔG in response to HBSS or RSL3 (0.5 μm; $n = 3$ biologically independent samples; *$P < 0.05$, two-way ANOVA with Tukey's multiple comparisons test; data are presented as means ± SD). (H) Image analysis of GFP/RFP puncta in indicated PANC1 cells following treatment with RSL3 (0.5 μM) for 12 h. The data are presented as box-and-whisker plots from 10 fields. Boxes represent the median and the 25th and 75th percentiles. *$P < 0.05$ versus control shRNA group, one-tailed *t* test; bar: 15 μm. (I, J) Immunoprecipitation (IP) analysis of the interaction between ATG5 and ATG16L1 in the indicated PANC1 cells following treatment with HBSS or RSL3. (K) Cell viability assay of indicated PANC1 cells following treatment with RSL3 (0.5 μm) for 3–24 h ($n = 3$ biologically independent samples; *$P < 0.05$, two-way ANOVA with Tukey's multiple comparisons test; data are presented as means ± SD). (L) Western blot analysis of protein expression in indicated MEFs following treatment with RSL3 (0.2 μM) for 12 h. (M) Cell viability assay of indicated PANC1 cells following treatment with RSL3 (0.5 μm) for 3–24 h in the absence or presence of 5 nM pyrrophenone (n = 3 biologically independent samples; *$P < 0.05$, two-way ANOVA with Tukey's multiple comparisons test; data are presented as means ± SD).

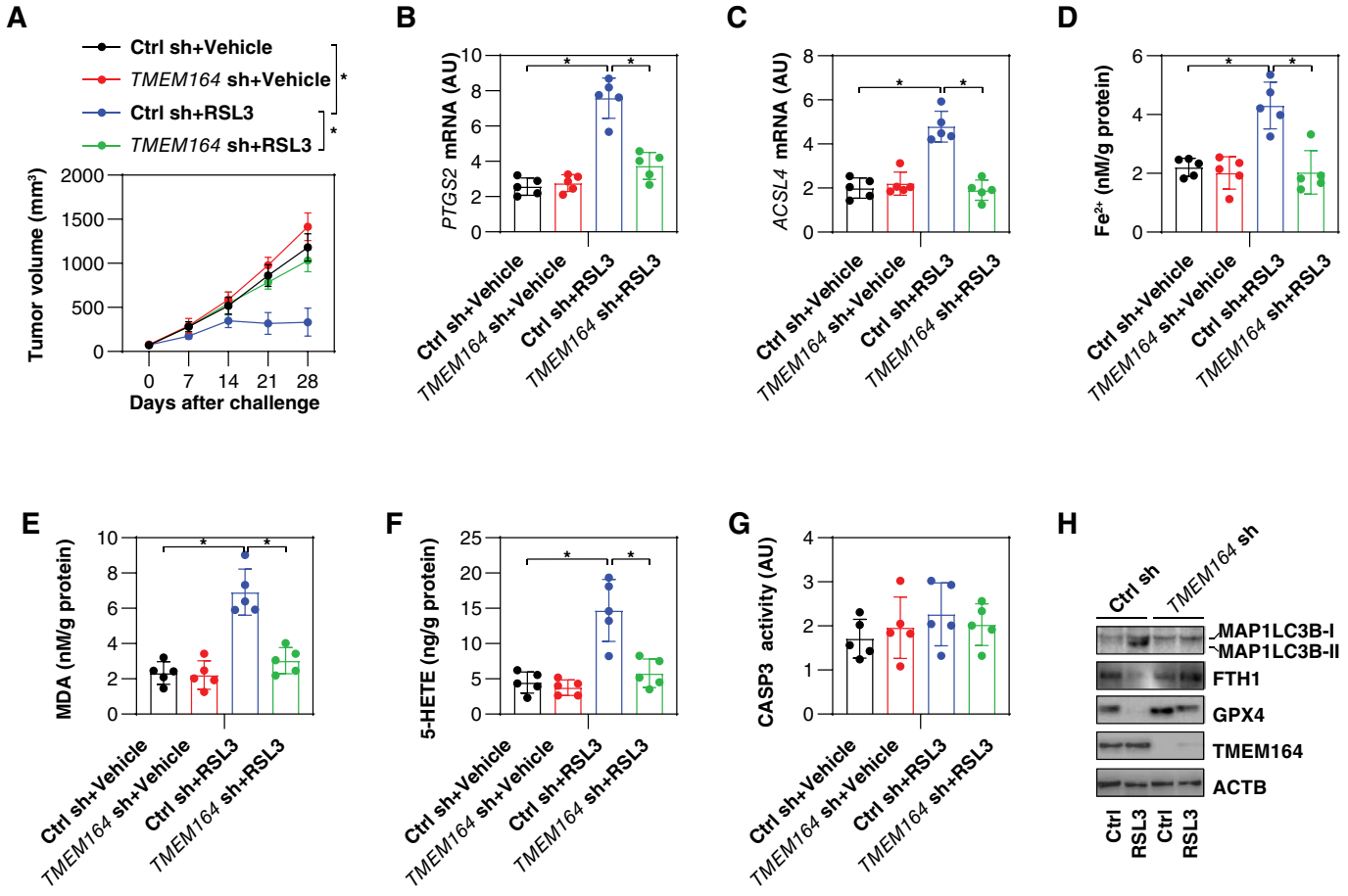

Figure 3. TMEM164 mediates the anticancer activity of RSL3 *in vivo*. (A) NOD SCID mice were injected subcutaneously with the indicated PANC1 cells (5×10^6/mouse) and treated with RSL3 (100 mg/kg, once every other day, intratumoral injection) at day 7 for 2 weeks. Tumor volume was calculated weekly ($n = 5$ mice/group; $^*P < 0.05$, ANOVA with Tukey's multiple comparisons test; data are presented as means ± SD). (B-H) in parallel, the activity or levels of *PTGS2* mRNA (B), *ACSL4* mRNA (C), Fe^{2+} (D), MDA (E), 5-HETE (F), CASP3 activity (G), and the indicated protein expression (H) in isolated tumors at day 28 were assayed ($n = 5$ mice/group; $^*P < 0.05$, ANOVA with Tukey's multiple comparisons test; data are presented as means ± SD). .

GPX4 (ab125066) were purchased from Abcam. The antibodies to AIFM2 (H00084883-D01P) and DHODH (14877-1-AP) were purchased from Thermo Fisher Scientific.

Cell culture

The HT1080 (CCL-121) and PANC1 (CRL-1469) cell lines were obtained from the American Type Culture Collection. The mouse pancreatic ductal adenocarcinoma cancer cell line KPC was a gift from David Tuveson (Cold Spring Harbor Laboratory). Wild-type and *atg5*$^{-/-}$ embryonic fibroblasts (MEFs) were a gift from Noboru Mizushima (Tokyo Medical and Dental University). Cell lines were cultured in Dulbecco's modified Eagle's medium (Thermo Fisher Scientific, 11995073) supplemented with 10% heat-inactivated fetal bovine serum (Millipore, TMS-013-B) and 1% penicillin and streptomycin (Thermo Fisher Scientific, 15070-063) at 37°C, 95% humidity, and 5% CO_2. The identity of the cell line was verified by short tandem repeat analysis, and routine mycoplasma testing was negative for contamination.

Animal models

Wild-type or TMEM164 KD PANC1 cells (5×10^6 cells) were injected subcutaneously into the dorsal side of NOD SCID mice (female, 8–10 weeks old). On the 7th day, these mice were given RSL3 (100 mg/kg, once every other day, intratumoral injection) for 2 weeks as previously described [44]. The diameter of the tumor was measured twice a week with a caliper, and the tumor volume was calculated using the following formula: length × width^2 × π/6. At 14 days after the injection, the mice were euthanized, and the xenograft solid tumors were collected.

All mice were maintained under specific pathogen-free conditions on a regular 12-h light and dark cycle (7:00-19:00 light period; room temperature 20°–25°C; relative humidity: 40%–60%). Food and water were available *ad libitum*. All animal experiments were conducted in accordance with the institutional ethics guidelines related to animal care and were approved by an institutional animal health and use committee.

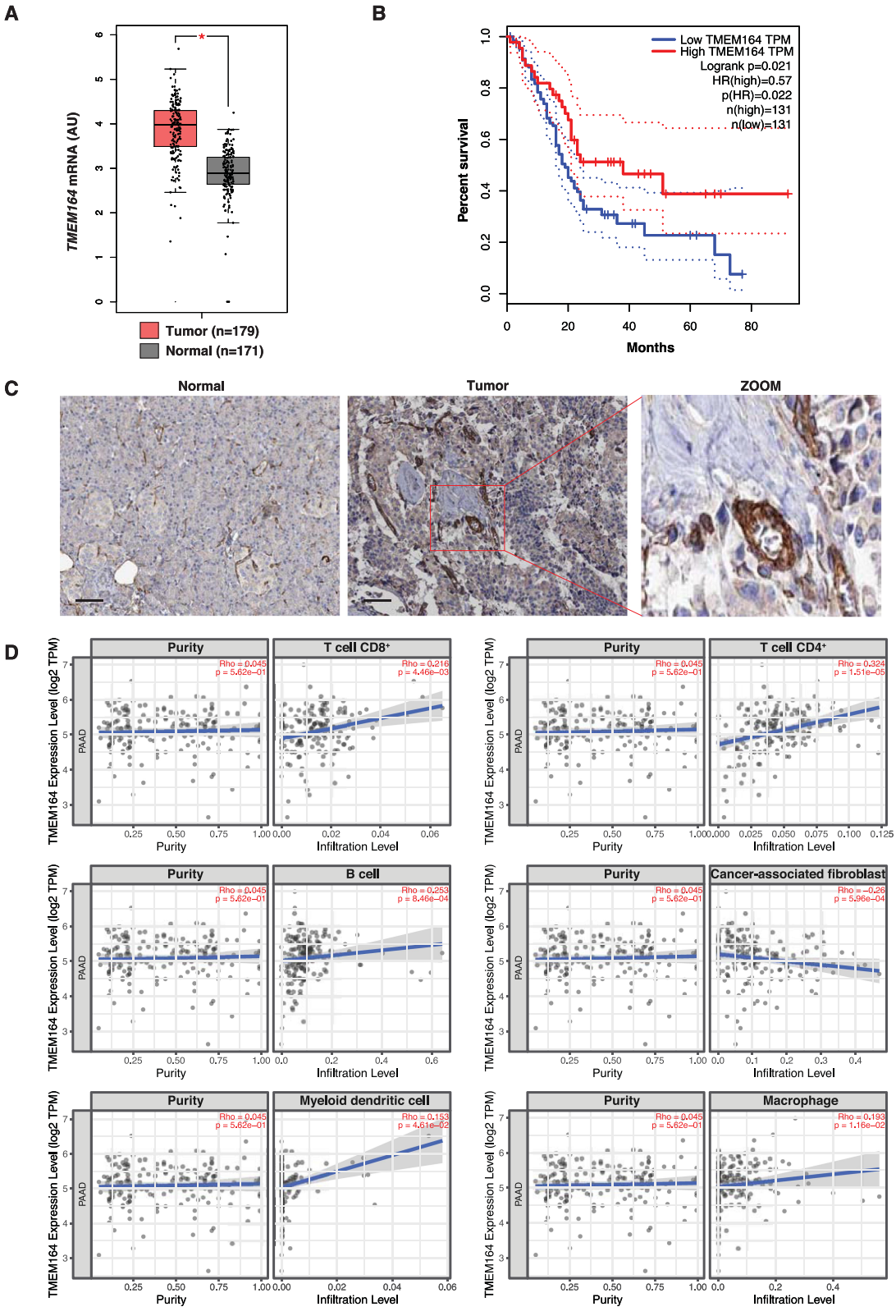

Figure 4. The role of TMEM164 in human pancreatic tumors. (A) Analysis of the gene expression of *TMEM164* in pancreas from tumor patients and normal controls using datasets from the Cancer Genome Atlas (TCGA; one-tailed *t* test). The data are presented as box-and-whisker plots. Boxes represent the median and the 25th and 75th percentiles. (B) Prognostic value of TMEM164 in human pancreatic cancer cohorts from the TCGA database. (C) Immunohistochemistry stains of TMEM164 in pancreas from tumor patients and normal controls from the Human Protein Atlas platform (bar=100 μm). (D) Analysis of the relationship between the gene expression of *TMEM164* and the immune cell infiltration in the pancreas of tumor patients using datasets from the Tumor IMmune Estimation Resource.

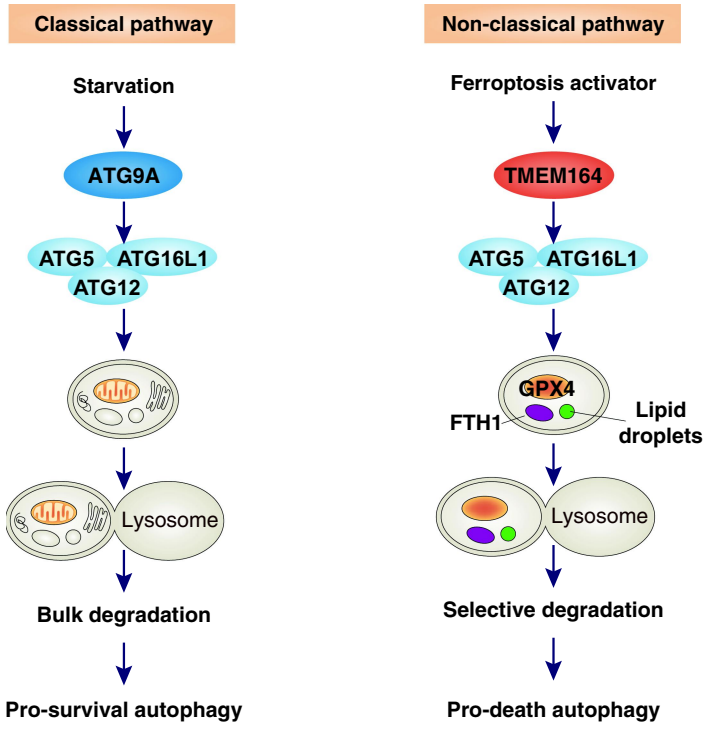

Figure 5. A model illustrating the role of TMEM164 in mediating autophagy-dependent cell death. ATG9A is required for starvation-induced autophagosome formation, which leads to programmed survival through non-selective degradation of cytosolic components. In contrast, a ferroptosis activator, such as RSL3, induces TMEM164-dependent autophagosome formation resulting in the selective degradation of anti-ferroptosis regulators (such as GPX4, FTH1, and lipid droplets).

Cytotoxicity assay

The level of cell death was assayed using a LIVE/DEAD cell viability/cytotoxicity assay kit (Thermo Fisher Scientific, L3224) according to the manufacturer's protocol.

Biochemical assay

Commercially available ELISA kits were used to measure the concentrations or activity of HMGB1 (Shino Test Corporation, ST51011), iron (Sigma-Aldrich, MAK025), MDA (Sigma-Aldrich, MAK085), lipid droplets (Cayman Chemical, 500001), 5-HETE (Abbexa, abx251443), and CASP3 (Cell Signaling Technology, 5723) in the indicated samples.

Autophagic flux analysis

We employed a GFP-LC3-RFP-LC3ΔG probe that was a gift from Noboru Mizushima (Addgene, 84572), which provides a simple and quantitative method to evaluate autophagic flux *in vitro* or *in vivo* [54]. In brief, cells (5000 cells/well) expressing GFP-LC3-RFP-LC3ΔG in a black 96-well plate with a clear bottom (Corning, 3904) were treated with RSL3 (0.5 μM) at the indicated times, and the signals of GFP and RFP were analyzed using a microplate reader (Tecan).

RNAi and gene transfection

The following human shRNAs were obtained from Sigma-Aldrich in a lentiviral format: human *TMEM164*-1 (TRCN0000122719), human *TMEM164*-2 (TRCN0000322570), mouse *Tmem164* (TRCN0000248887), human *ATG5* (TRCN0000151963), human *GPX4* (TRCN0000046249), human *FTH1* (TRCN0000029432), and human *ATG9A* (TRCN0000244083). We seeded 1×10^5 cells in each well of a 12-well plate in 500 μl of complete medium that were transduced by lentiviral vectors at a multiplicity of infection of 10:1. Transduction was carried out in the presence of polybrene (8 μg/ml; Thermo Fisher Scientific, TR1003 G) in an antibiotic-free medium. After recovering with complete culture medium, puromycin (5 μg/ml; Thermo Fisher Scientific, A1113802) was used for the selection of transduced cells. *TMEM164/Tmem164* cDNA was obtained from OriGene (SC105570 and MC207858) and gene transfection was performed by Lipofectamine 3000 (Thermo Fisher Scientific, L3000001).

qPCR

According to the manufacturer's instructions, we used a QIAGEN RNeasy Plus Micro Kit (74034) and iScript cDNA Synthesis Kit (Bio-Rad, 1708890) to extract total RNA and synthesize first-strand cDNA, respectively. Then, 20-μl reactions were prepared by combining 4 μl of iScript select reaction mix, 2 μl of gene-specific enhancer solution, 1 μl of reverse transcriptase, 1 μl of gene-specific assay pool (20×, 2 μM), and 12 μl of RNA diluted in RNase-free water. Quantitative real-time PCR (qPCR) was carried out using synthesized cDNA, primers, and SsoFast EvaGreen supermix (Bio-Rad, 172–5204). The primers were used as below: human

GPX4: 5'-ACAAGAACGGCTGCGTGGTGAA-3' and 5'-GCCACACACTTGTGGAGCTAGA-3'; human *PTGS2*: 5'-CGGTGAAACTCTGGCTAGACAG-3' and 5'-GCAAACCGTAGATGCTCAGGGA-3'; human *ACSL4*: 5'-GCTATCTCCTCAGACACACCGA-3' and 5'-AGGTGCTCCAACTCTGCCAGTA-3'; human *TMEM164*: 5'-AAGTTCGCCACCAAGACCGTCA-3' and 5'-GCTTGAAGACGACGATAGCTCC-3'; human *ACTB*: 5'-CACCATTGGCAATGAGCGGTTC-3' and 5'-AGGTCTTTGCGGATGTCCACGT-3'. The data were normalized to *ACTB* RNA, and the fold change was calculated via the $2^{-\Delta\Delta Ct}$ method [20]. Based on the untreated group, the relative concentration of mRNA was expressed in arbitrary units, and its assigned value was 1.

Western blot analysis

After treatment, whole cells were harvested and lysed at 4°C in ice-cold Cell Lysis Buffer (Cell Signaling Technology, 9803) containing a protease inhibitor cocktail (Thermo Fisher Scientific, 78429) [74]. A bicinchoninic acid (BCA) assay was used to detect protein concentration, and then 30 μg of protein in each lysate sample was subjected to SDS-PAGE (Bio-Rad, 3450124) at 100–120 V for 90 min, and then transferred to PVDF membrane (Bio-Rad, 1704273). The PVDF membrane was blocked with 5% nonfat dry milk (Cell Signaling Technology, 9999), and then incubated with the indicated primary antibody (1:500-1:1000) at 4°C overnight. The membrane was washed 3 times in tris-buffered saline Tween 20 (Cell Signaling Technology, 9997) buffer, and then incubated with an HRP-linked anti-mouse IgG secondary antibody (Cell Signaling Technology, 7076; 1:1000) or HRP-linked anti-rabbit IgG secondary antibody (Cell Signaling Technology, 7074; 1:1000) for 1 h at room temperature. After enhanced chemiluminescence exposure, a ChemiDoc Touch Imaging System (Bio-Rad, 1708370) or X-ray films were used for visualization and analysis of protein expression. ACTB was used as a housekeeping control for whole cell lysates.

Immunoprecipitation analysis

After treatment, the cells were lysed at 4°C using an ice-cold radio-immunoprecipitation assay lysis buffer (Millipore, 20–188), and the cell insoluble matter was removed by centrifugation (12,000 g, 10 min) [75]. BCA was used to detect the protein concentration, and then 300 μg of protein in each lysate sample was pre-cleared for 3 h with protein A/G Sepharose beads (Abcam, ab193262) at 4°C. Then, in the presence of protein A/G Sepharose beads, the sample with control IgG or a specific antibody (4 μg/mL) was gently shaken overnight at 4°C. After incubation, the protein A/G Sepharose beads were washed thoroughly with PBS, and the protein was eluted by boiling in 2 × Laemmli sample buffer (Bio-Rad, 161-0737) before SDS-PAGE electrophoresis.

Immunofluorescence analysis

Cells were cultured on glass coverslips and fixed in 3% formaldehyde for 30 min at room temperature prior to detergent extraction with 0.1% Triton X-100 (Cell Signaling Technology, 39487) for 10 min at 25°C. Coverslips were saturated with 2% bovine serum albumin (Cell Signaling Technology, 9998) in PBS for 1 h at room temperature and processed for immunofluorescence with MAP1LC3B antibody (1:200; Cell Signaling Technology, 3868), followed by Alexa Fluor 488-conjugated IgG (1:500; Thermo Fisher Scientific, A21206). Images were taken with a ZEISS LSM 800 confocal microscope. Relative quantitative colocalization analysis was performed from 10 random fields.

Bioinformatics analysis

The TCGA datasets, including gene expression and clinical outcomes data, were obtained from level 3 datasets at FireBrowse (http://gdac.broadinstitute.org; 2016 January). GEPIA (http://gepia.cancer-pku.cn/index.html), a developed interactive web server for analyzing the TCGA data, was used to separate the TCGA cohorts into groups with high/low expression of selected genes, which were then used for the prognostic signature validation. TIMER2.0 (http://timer.cistrome.org/), a web resource for systematic evaluations of the clinical impact of different immune cells in diverse cancer types, was used to assay the impact of the expression of TMEM164 on immune cell infiltration in patients with pancreatic ductal adenocarcinomas. The analysis of protein expression in human pancreatic cancer was based on The Human Protein Atlas online platform (http://www.proteinatlas.org/). In brief, the immunohistochemical staining of the indicated protein was used to yield a protein expression profile by the Human Protein Atlas consortium.

Statistical analysis

GraphPad Prism 8.4.3 was used to collect and analyze data. Unpaired Student's *t* tests were used to compare the means of two groups. A one-way or two-way analysis of variance (ANOVA) with Tukey's multiple comparisons test was used for comparison among the different groups. A *P* value of <0.05 was considered statistically significant.

Acknowledgments

We thank Dave Primm (Department of Surgery, University of Texas Southwestern Medical Center) for his critical reading of the manuscript. This work was partially supported by grants from the National Natural Science Foundation of China (81872323 and 82073299 to C.L.; 82172656 to X.Y.; 81830048 to J.L.).

Disclosure statement

No potential conflict of interest was reported by the author(s).

Funding

The author(s) reported there is no funding associated with the work featured in this article.

ORCID

Daolin Tang http://orcid.org/0000-0002-1903-6180

References

[1] Tang D, Chen X, Kang R, et al. Ferroptosis: molecular mechanisms and health implications. Cell Res. 2021;31(2):107–125. DOI:10.1038/s41422-020-00441-1

[2] Stockwell BR, Friedmann Angeli JP, Bayir H, et al. Ferroptosis: a regulated cell death nexus linking metabolism, redox biology, and disease. Cell. 2017;171(2):273–285. DOI:10.1016/j.cell.2017.09.021

[3] Chen X, Kang R, Kroemer G, et al. Broadening horizons: the role of ferroptosis in cancer. Nat Rev Clin Oncol. 2021;18(5):280–296. DOI:10.1038/s41571-020-00462-0

[4] Distefano AM, Martin MV, Cordoba JP, et al. Heat stress induces ferroptosis-like cell death in plants. J Cell Biol. 2017;216(2):463–476. DOI:10.1083/jcb.201605110

[5] Kuang F, Liu J, Kang R, et al. Oxidative damage and antioxidant defense in ferroptosis. Front Cell Dev Biol. 2020;8:586578. DOI:10.3389/fcell.2020.586578

[6] Chen X, Li J, Kang R, et al. Ferroptosis: machinery and regulation. Autophagy. 2021;17(9):2054–2081. DOI:10.1080/15548627.2020.1810918

[7] Xie Y, Hou W, Song X, et al. Ferroptosis: process and function. Cell Death Differ. 2016;23(3):369–379. DOI:10.1038/cdd.2015.158

[8] Dixon SJ, Lemberg KM, Lamprecht MR, et al. Ferroptosis: an iron-dependent form of nonapoptotic cell death. Cell. 2012;149(5):1060–1072. DOI:10.1016/j.cell.2012.03.042

[9] Klionsky DJ, Emr SD. Autophagy as a regulated pathway of cellular degradation. Science. 2000;290(5497):1717–1721. DOI:10.1126/science.290.5497.1717

[10] Dikic I, Elazar Z. Mechanism and medical implications of mammalian autophagy. Nat Rev Mol Cell Biol. 2018;19(6):349–364.

[11] Xie Y, Kang R, Sun X, et al. Posttranslational modification of autophagy-related proteins in macroautophagy. Autophagy. 2015;11(1):28–45. DOI:10.4161/15548627.2014.984267

[12] Hou W, Xie Y, Song X, et al. Autophagy promotes ferroptosis by degradation of ferritin. Autophagy. 2016;12(8):1425–1428. DOI:10.1080/15548627.2016.1187366

[13] Gao M, Monian P, Pan Q, et al. Ferroptosis is an autophagic cell death process. Cell Res. 2016;26(9):1021–1032.

[14] Park E, Chung SW. ROS-mediated autophagy increases intracellular iron levels and ferroptosis by ferritin and transferrin receptor regulation. Cell Death Dis. 2019;10(11):822.

[15] Rong Y, Fan J, Ji C, et al. USP11 regulates autophagy-dependent ferroptosis after spinal cord ischemia-reperfusion injury by deubiquitinating Beclin 1. Cell Death Differ. 2022;29(6):1164–1175. DOI:10.1038/s41418-021-00907-8

[16] Zhang Z, Guo M, Li Y, et al. RNA-Binding protein ZFP36/TTP protects against ferroptosis by regulating autophagy signaling pathway in hepatic stellate cells. Autophagy. 2020;16(8):1482–1505. DOI:10.1080/15548627.2019.1687985

[17] Xie Y, Kuang F, Liu J, et al. DUSP1 blocks autophagy-dependent ferroptosis in pancreatic cancer. J Pancreatology. 2020;3(3):154–160. DOI:10.1097/JP9.0000000000000054.

[18] Li C, Zhang Y, Liu J, et al. Mitochondrial DNA stress triggers autophagy-dependent ferroptotic death. Autophagy. 2021;17(4):948–960. DOI:10.1080/15548627.2020.1739447

[19] Liu K, Huang J, Liu J, et al. Induction of autophagy-dependent ferroptosis to eliminate drug-tolerant human retinoblastoma cells. Cell Death Dis. 2022;13(6):521. DOI:10.1038/s41419-022-04974-8

[20] Liu J, Zhu S, Zeng L, et al. DCN released from ferroptotic cells ignites AGER-dependent immune responses. Autophagy. 2021:1–14. DOI:10.1080/15548627.2021.2008692

[21] Kang R, Zhu S, Zeh HJ, et al. BECN1 is a new driver of ferroptosis. Autophagy. 2018;14(12):2173–2175. DOI:10.1080/15548627.2018.1513758

[22] Liu J, Kuang F, Kroemer G, et al. Autophagy-dependent ferroptosis: machinery and regulation. Cell Chem Biol. 2020;27(4):420–435. DOI:10.1016/j.chembiol.2020.02.005

[23] Zhou B, Liu J, Kang R, et al. Ferroptosis is a type of autophagy-dependent cell death. Semin Cancer Biol. 2020;66:89–100. DOI:10.1016/j.semcancer.2019.03.002

[24] Schmit K, Michiels C. TMEM proteins in cancer: a review. Front Pharmacol. 2018;9:1345.

[25] Gazou A, Riess A, Grasshoff U, et al. Xq22.3-Q23 deletion including ACSL4 in a patient with intellectual disability. Am J Med Genet A. 2013;161(4):860–864. DOI:10.1002/ajmg.a.35778

[26] Poreau B, Ramond F, Harbuz R, et al. Xq22.3q23 microdeletion harboring TMEM164 and AMMECR1 genes: two case reports confirming a recognizable phenotype with short stature, midface hypoplasia, intellectual delay, and elliptocytosis. Am J Med Genet A. 2019;179(4):650–654. DOI:10.1002/ajmg.a.61057

[27] Fan T, Liu Y, Liu H, et al. Transmembrane Protein-based risk model and H3K4me3 modification characteristics in lung adenocarcinoma. Front Oncol. 2022;12:828814.

[28] Zou Y, Palte MJ, Deik AA, et al. A GPX4-dependent cancer cell state underlies the clear-cell morphology and confers sensitivity to ferroptosis. Nat Commun. 2019;10(1):1617. DOI:10.1038/s41467-019-09277-9

[29] Doll S, Proneth B, Tyurina YY, et al. ACSL4 dictates ferroptosis sensitivity by shaping cellular lipid composition. Nat Chem Biol. 2017;13(1):91–98. DOI:10.1038/nchembio.2239

[30] Kagan VE, Mao G, Qu F, et al. Oxidized arachidonic and adrenic PEs navigate cells to ferroptosis. Nat Chem Biol. 2017;13(1):81–90. DOI:10.1038/nchembio.2238

[31] Yuan H, Li X, Zhang X, et al. Identification of ACSL4 as a biomarker and contributor of ferroptosis. Biochem Biophys Res Commun. 2016;478(3):1338–1343. DOI:10.1016/j.bbrc.2016.08.124

[32] Zou Y, Li H, Graham ET, et al. Cytochrome P450 oxidoreductase contributes tophospholipid peroxidation in ferroptosis. Nat Chem Biol. 2020;16(3):302–309. DOI:10.1038/s41589-020-0472-6

[33] Yan B, Ai Y, Sun Q, et al. Membrane damage during ferroptosis is caused by oxidation of phospholipids catalyzed by the oxidoreductases POR and CYB5R1. Mol Cell. 2020. DOI:10.1016/j.molcel.2020.11.024.

[34] Yamaguchi Y, Kasukabe T, Kumakura S. Piperlongumine rapidly induces the death of human pancreatic cancer cells mainly through the induction of ferroptosis. Int J Oncol. 2018;52(3):1011–1022.

[35] Eling N, Reuter L, Hazin J, et al. Identification of artesunate as a specific activator of ferroptosis in pancreatic cancer cells. Oncoscience. 2015;2(5):517–532.

[36] Liu Y, Wang Y, Liu J, et al. Interplay between MTOR and GPX4 signaling modulates autophagy-dependent ferroptotic cancer cell death. Cancer Gene Ther. 2021;28(1–2):55–63. DOI:10.1038/s41417-020-0182-y

[37] Zhu S, Zhang Q, Sun X, et al. HSPA5 regulates ferroptotic cell death in cancer cells. Cancer Res. 2017;77(8):2064–2077. DOI:10.1158/0008-5472.CAN-16-1979

[38] Xie Y, Zhu S, Zhong M, et al. Inhibition of aurora kinase a induces necroptosis in pancreatic carcinoma. Gastroenterology. 2017;153(5):1429–43 e5. DOI:10.1053/j.gastro.2017.07.036

[39] Dai C, Chen X, Li J, et al. Transcription factors in ferroptotic cell death. Cancer Gene Ther. 2020;27(9):645–656. DOI:10.1038/s41417-020-0170-2

[40] Dodson M, Castro-Portuguez R, Zhang DD. NRF2 plays a critical role in mitigating lipid peroxidation and ferroptosis. Redox Biol. 2019;23:101107.

[41] Sun X, Ou Z, Chen R, et al. Activation of the p62-Keap1-NRF2 pathway protects against ferroptosis in hepatocellular carcinoma cells. Hepatology. 2016;63(1):173–184. DOI:10.1002/hep.28251

[42] Olayanju A, Copple IM, Bryan HK, et al. Brusatol provokes a rapid and transient inhibition of Nrf2 signaling and sensitizes mammalian cells to chemical toxicity-implications for therapeutic targeting of Nrf2. Free Radic Biol Med. 2015;78:202–212.

[43] Wen Q, Liu J, Kang R, et al. The release and activity of HMGB1 in ferroptosis. Biochem Biophys Res Commun. 2019;510(2):278–283. DOI:10.1016/j.bbrc.2019.01.090
[44] Yang WS, SriRamaratnam R, Welsch ME, et al. Regulation of ferroptotic cancer cell death by GPX4. Cell. 2014;156(1–2):317–331. DOI:10.1016/j.cell.2013.12.010
[45] Doll S, Freitas FP, Shah R, et al. FSP1 is a glutathione-independent ferroptosis suppressor. Nature. 2019;575(7784):693–698. DOI:10.1038/s41586-019-1707-0
[46] Bersuker K, Hendricks JM, Li Z, et al. The CoQ oxidoreductase FSP1 acts parallel to GPX4 to inhibit ferroptosis. Nature. 2019;575(7784):688–692. DOI:10.1038/s41586-019-1705-2
[47] Mao C, Liu X, Zhang Y, et al. DHODH-Mediated ferroptosis defence is a targetable vulnerability in cancer. Nature. 2021;593(7860):586–590. DOI:10.1038/s41586-021-03539-7
[48] Wu Z, Geng Y, Lu X, et al. Chaperone-mediated autophagy is involved in the execution of ferroptosis. Proc Natl Acad Sci USA. 2019;116(8):2996–3005. DOI:10.1073/pnas.1819728116
[49] Bai Y, Meng L, Han L, et al. Lipid storage and lipophagy regulates ferroptosis. Biochem Biophys Res Commun. 2019;508(4):997–1003. DOI:10.1016/j.bbrc.2018.12.039
[50] Klionsky DJ, Abdel-Aziz AK, Abdelfatah S, et al. Guidelines for the use and interpretation of assays for monitoring autophagy (1). Autophagy. 2021;17:1–382. DOI:10.1080/15548627.2020.1797280
[51] Judith D, Jefferies HBJ, Boeing S, et al. ATG9A shapes the forming autophagosome through Arfaptin 2 and phosphatidylinositol 4-kinase IIIβ. J Cell Biol. 2019;218(5):1634–1652.
[52] Noda T, Kim J, Huang WP, et al. Apg9p/cvt7p is an integral membrane protein required for transport vesicle formation in the Cvt and autophagy pathways. J Cell Biol. 2000;148(3):465–480. DOI:10.1083/jcb.148.3.465
[53] Lang T, Reiche S, Straub M, et al. Autophagy and the cvt pathway both depend on AUT9. J Bacteriol. 2000;182(8):2125–2133.
[54] Kaizuka T, Morishita H, Hama Y, et al. An autophagic flux probe that releases an internal control. Mol Cell. 2016;64(4):835–849. DOI:10.1016/j.molcel.2016.09.037
[55] Mizushima N, Noda T, Yoshimori T, et al. A protein conjugation system essential for autophagy. Nature. 1998;395(6700):395–398. DOI:10.1038/26506
[56] Suzuki K, Kirisako T, Kamada Y, et al. The pre-autophagosomal structure organized by concerted functions of APG genes is essential for autophagosome formation. Embo J. 2001;20(21):5971–5981.
[57] Zhang I, Cui Y, Amiri A, et al. Pharmacological inhibition of lipid droplet formation enhances the effectiveness of curcumin in glioblastoma. Eur J Pharm Biopharm. 2016;100:66–76.
[58] Chen X, Kang R, Kroemer G, et al. Ferroptosis in infection, inflammation, and immunity. J Exp Med. 2021;218(6):e20210518. DOI:10.1084/jem.20210518
[59] Jung S, Jeong H, Yu SW. Autophagy as a decisive process for cell death. Exp Mol Med. 2020;52(6):921–930.
[60] Kroemer G, Levine B. Autophagic cell death: the story of a misnomer. Nat Rev Mol Cell Biol. 2008;9(12):1004–1010.
[61] Galluzzi L, Vitale I, Aaronson SA, et al. Molecular mechanisms of cell death: Recommendations of the nomenclature committee on cell death 2018. Cell Death Differ. 2018;25:486–541.
[62] Li J, Liu J, Xu Y, et al. Tumor heterogeneity in autophagy-dependent ferroptosis. Autophagy. 2021;17(11):3361–3374. DOI:10.1080/15548627.2021.1872241
[63] Yang M, Chen P, Liu J, et al. Clockophagy is a novel selective autophagy process favoring ferroptosis. Sci Adv. 2019;5(7):eaaw2238. DOI:10.1126/sciadv.aaw2238
[64] Chen X, Song X, Li J, et al. Identification of HPCAL1 as a specific autophagy receptor involved in ferroptosis. Autophagy. 2022;1–21. DOI:10.1080/15548627.2022.2059170
[65] Zhang Y, Swanda RV, Nie L, et al. mTORC1 couples cyst(e)ine availability with GPX4 protein synthesis and ferroptosis regulation. Nat Commun. 2021;12(1):1589. DOI:10.1038/s41467-021-21841-w
[66] Han L, Bai L, Fang X, et al. SMG9 drives ferroptosis by directly inhibiting GPX4 degradation. Biochem Biophys Res Commun. 2021;567:92–98. DOI:10.1016/j.bbrc.2021.06.038
[67] Guardia CM, Christenson ET, Zhou W, et al. The structure of human ATG9A and its interplay with the lipid bilayer. Autophagy. 2020;16(12):2292–2293. DOI:10.1080/15548627.2020.1830522
[68] Dai E, Han L, Liu J, et al. Ferroptotic damage promotes pancreatic tumorigenesis through a TMEM173/STING-dependent DNA sensor pathway. Nat Commun. 2020;11(1):6339. DOI:10.1038/s41467-020-20154-8
[69] Lang X, Green MD, Wang W, et al. Radiotherapy and immunotherapy promote tumoral lipid oxidation and ferroptosis via synergistic repression of SLC7A11. Cancer Discov. 2019;9(12):1673–1685. DOI:10.1158/2159-8290.CD-19-0338
[70] Jiang L, Kon N, Li T, et al. Ferroptosis as a p53-mediated activity during tumour suppression. Nature. 2015;520(7545):57–62. DOI:10.1038/nature14344
[71] Wang W, Green M, Choi JE, et al. CD8(+) T cells regulate tumour ferroptosis during cancer immunotherapy. Nature. 2019;569(7755):270–274. DOI:10.1038/s41586-019-1170-y
[72] Wu J, Minikes AM, Gao M, et al. Intercellular interaction dictates cancer cell ferroptosis via NF2–YAP signalling. Nature. 2019;572(7769):402–406. DOI:10.1038/s41586-019-1426-6
[73] Lei G, Zhang Y, Koppula P, et al. The role of ferroptosis in ionizing radiation-induced cell death and tumor suppression. Cell Res. 2020;30(2):146–162. DOI:10.1038/s41422-019-0263-3
[74] Dai E, Han L, Liu J, et al. Autophagy-dependent ferroptosis drives tumor-associated macrophage polarization via release and uptake of oncogenic KRAS protein. Autophagy. 2020;16(11):2069–2083. DOI:10.1080/15548627.2020.1714209
[75] Tang D, Kang R, Livesey KM, et al. Endogenous HMGB1 regulates autophagy. J Cell Biol. 2010;190(5):881–892. DOI:10.1083/jcb.200911078